SERBIAN JOURNAL OF ELECTRICAL ENGINEERING
Vol. 12, No. 1, February 2015, 33–52

UDC: 621.314.2:621.3.013.1 **DOI: 10.2298/SJEE1501033P**

The Theorem about the Transformer Excitation Current Waveform Mapping into the Dynamic Hysteresis Loop Branch for the Sinusoidal Magnetic Flux Case

Nenad Petrović[1], Velibor Pjevalica[2], Vladimir Vujičić[3]

Abstract: This paper analyses aspects of the approximation theory application on the certain subsets of the measured samples of the transformer excitation current and the sinusoidal magnetic flux. The presented analysis is performed for single-phase transformer case, Epstein frame case and toroidal core case. In the paper the theorem of direct mapping the transformer excitation current in the stationary regime is proposed. The excitation current is mapped to the dynamic hysteresis loop branch (in further text DHLB) by an appropriate cosine transformation. This theorem provides the necessary and satisfactory conditions for above described mapping. The theorem highlights that the transformer excitation current under the sinusoidal magnetic flux has qualitatively equivalent information about magnetic core properties as the DHLB. Furthermore, the theorem establishes direct relationship between the number of the transformer excitation current harmonics and their coefficients with the degree of the DHLB interpolation polynomial and its coefficients. The DHLB interpolation polynomial is calculated over the measured subsets of samples representing Chebyshev nodes of the first and the second kind. These nonequidistant Chebyshev nodes provides uniform convergence of the interpolation polynomial to the experimentally obtained DHLB with an excellent approximation accuracy and are applicable on the approximation of the static hysteresis loops and the DC magnetization curves as well.

Keywords: Excitation Transformer Current, Dynamic Hysteresis Loop, Sinusoidal Magnetic Flux, Approximation, Chebyshev nodes.

1 Introduction

Different approaches to the magnetic hysteresis modeling have been researched and developed over the last century. The study of the hysteresis

[1]Nenad Petrović is with the School of Electrical Engineering Stari grad, 37 Visokog Stevana, 11000 Belgrade, Serbia; E-mail: nploewenstein@ gmail.com
[2]Velibor Pjevalica is with the JP Srbijagas, Technical Provision Section, 12 Narodnog fronta, 21000 Novi Sad, Serbia; E-mail: velibor.pjevalica@srbijagas.com
[3]Vladimir Vujičić is with the Faculty of Technical Sciences, University of Novi Sad, 6 Trg D. Obradovića, 21000 Novi Sad, Serbia**;** E-mail: vujicicv@uns.ac.rs

phenomenon has been oriented towards a detailed experimental research and observation (Ewing [1], Madelung [2]) from the very onset. At the same time, significant endeavors have been made to find such mathematical expressions that would accurately describe magnetic curve upon certain physical parameters (Langevin [3], Brillouin [4]). This idea has been further developed in the works of Preisach [5] and Jiles-Atherton [6].

From the point of view of engineering, an approach based on fitting the experimentally obtained magnetic curve data with the properly chosen approximation function was applied in the works of Fisher and Moser [7], Trutt and Erdélyi [8], Widger [9], Brauer [10], Rivas, Zamarro, Martin and Pereira [11].

But, after Jiles-Atherton method was published, over the last three decades the researchers have mostly focused on the comparative study, systematization and improvement of Preisach's [5] and Jiles-Atherton's [6] hysteresis models in the works of Mayergoyz [12], Bertotti [13], Iványi [14], Della Torre [15], Takács [16], and other authors mostly referenced in the above-mentioned works. In the process of searching for optimal mathematical models of hysteresis curves, the idea of representing the entire major hysteresis loop by a single function, mostly because of the unsatisfactory accuracy and computation efficiency, was somehow pushed aside.

The basic idea of this work draws upon the property of discrete orthogonality of the Chebyshev polynomials [17, 18] over the subsets of the excitation transformer current and the sinusoidal magnetic flux samples that represent Chebyshev nodes of the first (CHN_I) and the second kind (CHN_II) [18]. This property provides that an algebraic form of the DHLB approximation polynomial can be represented as a sum of products of the Chebyshev polynomials and the coefficients computed by using discrete Fourier transformation (DFT) over the sample subsets CHN_I and CHN_II [18]. Actually, the trigonometric cosine interpolation polynomial [19] of the transformer excitation current is generated in the same way. Section 5 looks at the existence of the sample subsets CHN_I and CHN_II, depending on the applied sampling system.

This is the main advantage over all proposed approximations [7 – 11] in terms of both accuracy and computing efficiency. The fact that the coefficients of discrete Chebyshev and Fourier transformation over the subsets CHN_I and CHN_II are equivalent [18] enables uniform convergence of the interpolation polynomial to the experimentally obtained DHLB in the same way as the trigonometric cosine polynomial uniform converge to the excitation transformer current. Consequently, both the accuracy and the computation efficiency are on the level of discrete Fourier transformation. This topic is considered in Section 5.

With the equivalent level of accuracy, a single approximation function in the form of the interpolation polynomial has an obvious advantage in computation

efficiency over the representation of the major dynamic hysteresis loop proposed in [7 – 11] or over the representation by splines.

The relations among relevant magnitudes are presented in Section 2. Section 3 contains mathematical conditions that must be fulfilled for a good quality approximation. The theorem is presented in Section 4. Section 5 discusses the practical aspects of the given theorem. Section 6 contains conclusions and guidelines for the future research.

2 Relations among relevant magnitudes

The relation between the single-phase transformer/Epstein frame input voltage, excittation current and magnetic flux by virtue of the II Kirchhoff law is given by

$$u_1(t) = R_1 i_0(t) + L_{\sigma 1} \frac{\mathrm{d}\, i_0(t)}{\mathrm{d}\, t} + N_1 \frac{\mathrm{d}\, \varphi(t)}{\mathrm{d}\, t}, \tag{1}$$

where R_1 is resistance of the primary winding, $L_{\sigma 1}$ is leakage reactance of the primary winding, $u_1(t)$ is input voltage, $i_0(t)$ is excitation current, N_1 – number of turns in the primary winding, $\varphi(t)$ – time-domain function of the single turn flux in the magnetic core and $e(t) = \mathrm{d}\varphi(t)/\mathrm{d}t$ – electromotive force (EMF) induced in the single turn of either primary or secondary winding. Since the magnetic core is made of the ferromagnetic material, the function $\varphi(i_0)$ is nonlinear. Due to the nonlinearity of the function $\varphi(i_0)$ i.e. $i_0(\varphi)$, the excitation current $i_0(t)$ will be nonsinusoidal and thus the sinusoidal excitation $u_1(t)$ will produce the nonsinusoidal response given by

$$N_1 \frac{\mathrm{d}\, \varphi(t)}{\mathrm{d}\, t} = u_1(t) - \left(R_1 i_0(t) + L_{\sigma 1} \frac{\mathrm{d}\, i_0(t)}{\mathrm{d}\, t} \right). \tag{2}$$

Because of the nonsinusoidal first derivative $\mathrm{d}\varphi(t)/\mathrm{d}t$ of the periodic function $\varphi(t)$, it follows that $\varphi(t)$ is nonsinusoidal as well. However, relevant references [20, 21] treat the computation of EMF induced in the single turn of the transformer winding assuming that the magnetic flux $\varphi(t)$ in the given magnetic core is sinusoidal. Similarly, the magnetic flux $\varphi(t)$ is treated in the standards for Epstein frame measurement [22, 23] and measurements based on the Epstein frame principle [24]. This is done for practical reasons which are explained in the following section.

3 Conditions for Magnetic Flux Approximation with Sine Wave Function in the Time Domain

3.1 Conditions

The term of the equation (2) given by

$$R_1 i_{1n}(t) + L_{\sigma 1}\,\mathrm{d}i_{1n}(t)/\mathrm{d}t \tag{3}$$

with the rated transformer current I_{1n} does not exceed values of the short circuit voltage [21], which is about 10^{-2} times the order of magnitude of the input voltage $u_1(t)$. In particular: $R_1 i_{1n}(t) + L_{\sigma 1}\mathrm{d}i_{1n}(\mathrm{t})/\mathrm{d}t \sim 10^{-2} u_1(t)$. The same statement holds to the ratio between the excitation and the rated transformer current magnitude: $i_0(t) \sim 10^{-2} i_{1n}(t)$ [21]. Thus, for the magnitude of the term $R_1 i_0(t) + L_{\sigma 1}\mathrm{d}i_0(t)/\mathrm{d}t$ in (1) holds:

$$R_1 i_0(t) + L_{\sigma 1}\,\mathrm{d}i_0(t)/\mathrm{d}t \sim 10^{-4} u_1(t), \tag{4}$$

so it can be neglected and the equation (1) can be approximated as

$$N_1\,\mathrm{d}\varphi(t)/\mathrm{d}t = -N_1 e(t) = u_1(t). \tag{5}$$

The equation (5) shows that the magnetic flux in the single-phase transformer, Epstein frame and toroidal core specimen in the stationary regime with the sinusoidal input voltage $u_1(t)$ can be treated as a pure sine wave.

3.2 Excitation current in excitation winding and sine wave magnetic flux relation

Taking into account previous ascertainment, the reference [20] gives mutual relationship between the excitation current and the magnetic flux in the form known as the dynamic hysteresis loop (illustrated in Fig. 1.11 [20]).

This one dynamic hysteresis loop, that is symmetric to the origin $i_0 - \varphi$, implies that the extreme values of the magnetic flux and the excitation current comes together (synchronously).

Based on the two above analyzed conditions: 1 – sinusoidal magnetic flux in the magnetic core and 2 – synchronous appearance of the extreme values of the magnetic flux and the excittation current with addition of the condition 3 – that the excitation current $i_0(t)$ between its consecutive negative and positive extreme values is strictly monotonic, the theorem about mapping the excitation current $i_0(t)$ from the time (or electric angle $\theta = \omega t$) segment between its consecutive negative and positive (or vice versa) extreme values, to the dynamic hysteresis loop branch $i_0(\varphi)$ onto normalized segment of the magnetic flux values $\varphi \in [-1,1]$, can be derived.

4 The Theorem

Theorem I

Let $i_0(\theta) \in C[-\pi,0]$ to be an excitation current function of the electric angle domain variable in the primary (excitation) winding of transformer or Epstein frame that satisfies the conditions

$$\min_{-\pi\le\theta\le 0} i_0(\theta) = -\max_{-\pi\le\theta\le 0}\left|i_0(\theta)\right| = -I_m = i_0(-\pi),$$
$$\max_{-\pi\le\theta\le 0} i_0(\theta) = \max_{-\pi\le\theta\le 0}\left|i_0(\theta)\right| = I_m = i_0(0), \tag{6}$$

$$i_0(\theta_1) < i_0(\theta_2), \quad -\pi \le \theta_1 < \theta_2 \le 0. \tag{7}$$

and let $\varphi \in C[-\pi,\pi]$ to be the sinusoidal magnetic flux function of the electric angle in the transformer/Epstein frame magnetic core across the excitation winding that satisfies the condition

$$\min_{-\pi\le\theta\le 0} \varphi(\theta) = \varphi(-\pi) = -1, \quad \max_{-\pi\le\theta\le 0} \varphi(\theta) = \varphi(0) = 1. \tag{8}$$

Then the mapping $i_0(\cos\theta) = i_0(\theta)$ represents the dynamic hysteresis loop branch function $i_0(\varphi)$ of the magnetic flux domain variable: $i_0(\varphi)\in C[-1,1]$, $i_0(\varphi)\in[-I_m, I_m]$. The functions $i_0(\theta)$ and $\varphi(\theta)$ satisfying conditions of the Theorem I are shown in Fig. 1.

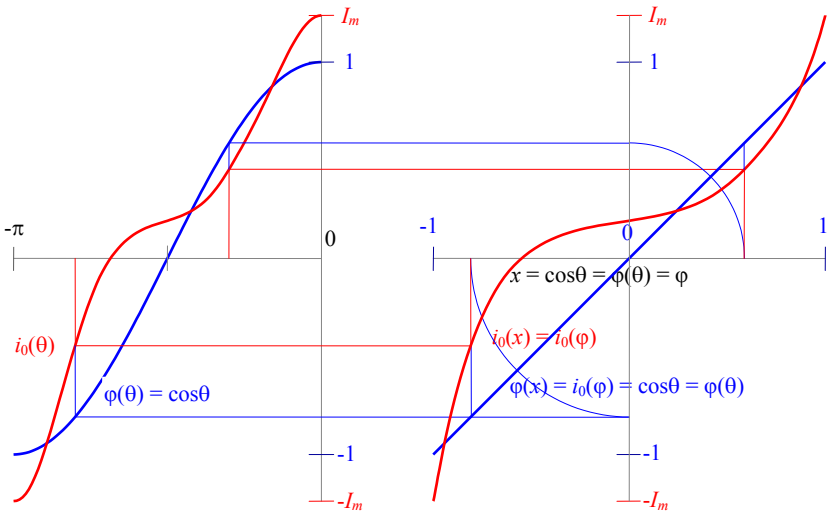

Fig. 1 – (a) *Waveforms of excitation current and magnetic flux satisfying the Theorem I conditions;* (b) *Process of excitation current mapping into hysteresis loop branch.*

Note 1: Notation $i_0(\theta)\in C[-\pi,0]$ means that the function $i_0(\theta)$ belongs to the class of continuous functions on the segment $\theta\in[-\pi,0]$ and $i_0(\varphi)$ belongs to the class of continuous functions on the segment $\varphi\in[-1,1]$.

Note 2: Not losing in generality, the function $\varphi\in[-1,1]$ is normalized so the proof for the case of arbitrary amplitude values $\varphi\in[-\Phi_m, \Phi_m]$ is given in the corollary bellow.

Proof

The considered function $i_0(\theta)\in C[-\pi,0]$, which meets the conditions (6) and (7), belongs to the general class of periodic functions $i_0(2\pi ft)\in C[2\pi ft, 2\pi ft+T] = C^0_{2\pi}$. The sinusoidal magnetic flux belongs to this class as well: $\varphi(2\pi ft)\in C[2\pi ft, 2\pi ft+T] = C^0_{2\pi}$. The extreme values of the same sign of these two functions are simultaneous in time $t+kT/2$, $k\in N$, which is the reason that these two functions can be treated in the class of the functions $i_0(\theta)$, $\varphi(\theta)\in C[-\pi,\pi]$ whose extreme values of the same sign are simultaneous for the next variable θ values: $\{-\pi,0,\pi\}$. Let select these values as

$$i_0(-\pi) = -I_m, \quad i_0(0) = I_m, \quad i_0(\pi) = -I_m,$$

and

$$\varphi(-\pi) = -1, \quad \varphi(0) = 1, \quad \varphi(\pi) = -1,$$

in such way that compliance with the conditions (6) and (8) is ensured. Then, based on the assumption that $\varphi(\theta)\in C[-\pi,\pi]$ is a sinusoidal function, it follows that $\varphi(\theta) = \cos\theta$.

The functions $i_0(\theta)$ and $\varphi(\theta)$ are given parametrically. Since the analytical form of the function $i_0(\theta)$ is unknown, it is necessary to find a new parameter function $x(\theta)$ so that is $\varphi(\theta^{-1}(x)) = x(\theta^{-1}(\varphi))$. In such way a linear dependence $\varphi(x) = x(\varphi)$ (Fig. 1) is established, which further allows direct derivation of the function $i_0(\varphi)$ starting from the new parametric form of the function $i_0(x)$ and $\varphi(x)$.

By mapping of the segment $\theta\in[-\pi,0]$ into the segment $x\in[-1,1]$ using the function $x = \cos\theta$ (Fig. 1), the monotonic function $i_0(\theta)\in[-I_m, I_m]$, based on (7), is uniquely transformed into a new monotonic function

$$i_0(\cos\theta) = i_0(x)\in[-I_m, I_m], \tag{9}$$

so that holds

$$\begin{aligned} &i_0(\theta_1) = i_0(\cos\theta_1) = i_0(x_1) < i_0(\theta_2) = i_0(\cos\theta_2) = i_0(x_2), \\ &-\pi \le \theta_1 < \theta_2 \le 0, \qquad 1 \le \cos\theta_1 = x_1 < \cos\theta_2 = x_2 \le 1. \end{aligned} \tag{10}$$

Also, the mapping of the segment $\theta\in[-\pi,0]$ into the segment $x\in[-1,1]$ using the function $x = \cos\theta$ (Fig. 1), the cosine magnetic flux function $\varphi(\theta) = \cos\theta\in[-1,1]$ is transformed into a linear function $\varphi(x) = \cos(\arccos x) = x$. This function actually is the Chebyshev polynomial of the first kind $T_1(x) = x$, so that its inverse function (Fig. 1) is

$$\varphi^{-1}(x) = x(\varphi) = \varphi, \qquad x(\varphi) \in [-1,1], \qquad \varphi \in [-1,1]. \tag{11}$$

Based on equations (10) and (11) it follows that

$$i_0(\theta) = i_0(\cos\theta) = i_0(x) = i_0(\varphi),$$
$$-\pi \le \theta_1 < \theta_2 \le 0, \qquad 1 \le \cos\theta_1 = x_1 = \varphi_1 < \cos\theta_2 = x_2 = \varphi_2 \le 1$$

which statement was to be proved. ■

The steps in proving the theorem and the result of the theorem are graphically shown in Fig. 1.

When the extreme values of the magnetic flux function deviate from the unit values, but meet the condition

$$\begin{aligned} \min_{-\pi\le\theta\le 0} \varphi(\theta) &= -\max_{-\pi\le\theta\le 0} |\varphi(\theta)| = -\Phi_m = \varphi(-\pi), \\ \max_{-\pi\le\theta\le 0} \varphi(\theta) &= \max_{-\pi\le\theta\le 0} |\varphi(\theta)| = \Phi_m = \varphi(0), \end{aligned} \tag{12}$$

the following corollary reformulates the Theorem I:

Corollary I

If the condition (8) of the Theorem I is replaced with the condition (12), then the mapping $i_0(\Phi_m\cos\theta) = i_0(\theta)$ represents the dynamic hysteresis loop branch function $i_0(\varphi)$ of the magnetic flux variable: $i_0(\varphi) \in C[-\Phi_m, \Phi_m]$, $i_0(\varphi) \in [-I_m, I_m]$.

Note 3: Notation $i_0(\varphi) \in C[-\Phi_m, \Phi_m]$ means that the function $i_0(\varphi)$ belongs to the class of continuous functions on the closed variable interval $\varphi \in [-\Phi_m, \Phi_m]$.

Proof

When the amplitude of the sinusoidal magnetic flux deviates from the unit values, the function of the magnetic flux takes the form

$$\varphi(\theta) = \Phi_m \cos\theta. \tag{13}$$

The segment $\theta \in [-\pi,0]$ will be now uniquely mapped to the segment $x \in [-\Phi_m, \Phi_m]$ by the parameter function $x = \varphi(\theta) = \Phi_m\cos\theta$, so the cosine function of the magnetic flux $\varphi(\theta) = \Phi_m\cos\theta \in [-\Phi_m, \Phi_m]$ will be transformed into a linear function $\varphi(x) = \Phi_m\cos(\arccos(x/\Phi_m)) = \Phi_m T_1(x/\Phi_m) = x$, and its inverse function takes the form

$$\varphi^{-1}(x) = x(\varphi) = \varphi, \qquad x(\varphi) \in [-\Phi_m, \Phi_m], \qquad \varphi \in [-\Phi_m, \Phi_m]. \tag{14}$$

Based on (8) and (15) it follows that

$$i_0(\theta) = i_0(\Phi_m \cos\theta) = i_0(x) = i_0(\varphi), \quad -\pi \le \theta_1 < \theta_2 \le 0,$$
$$-\Phi_m \le \Phi_m \cos\theta_1 = x_1 = \varphi_1 < \Phi_m \cos\theta_2 = x_2 = \varphi_2 \le \Phi_m,$$

which statement was to be proved. ■

The result of the Corollary 1 is graphically shown in Fig. 2.

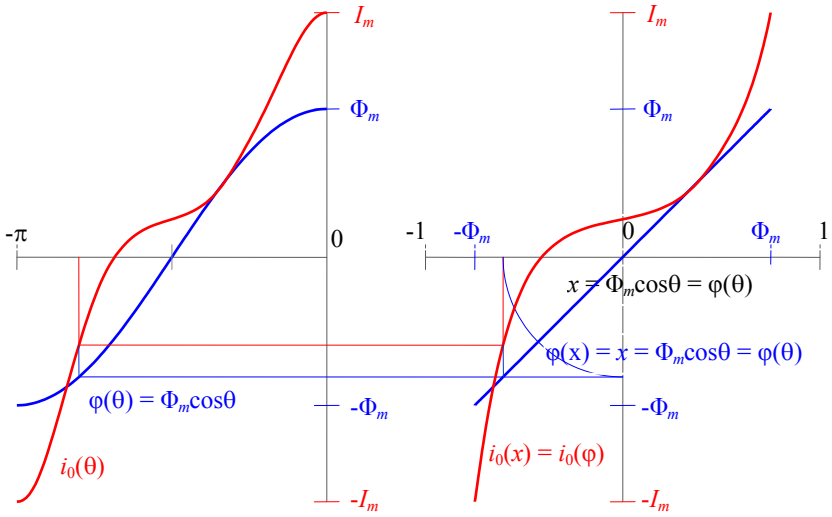

Fig. 2 – *The process of excitation current mapping into hysteresis loop branch for arbitrary magnetic flux amplitude value.*

Note 4: The magnetic flux in certain operating conditions, particularly during the transition process, is not a sinusoidal function of time. The Theorem I does not apply in such cases, neither the Corollary I.

5 Discussion

1. The Theorem I, along with its Corollary I, shows that the excitation winding current characterizes qualitatively in the same way the behavior of a magnetic circuit under sinusoidal magnetic flux just as its hysteresis loop branch does.
2. The Theorem I and its Corollary I do not determines the analytical dependence of the above-mentioned functions of physical processes in the magnetic circuit, but determines the conditions under which the results of approximation theory [17 – 19] can be precisely applied. In particular, this means the following:

The mapping of the segment $[-\pi,0]$ on $[-1,1]$ by using the parametric function $x = \cos\theta$ ($\theta = 2\pi t/T$) the functions $\cos(k\theta)$, $k = 0,\ldots,n$ defined on the segment $[-\pi,0]$ are transformed into the Chebyshev polynomials of the first kind $T_1(x) = \cos(k(\arccos x))$, $k = 0,\ldots,n$, on the segment $[-1,1]$, which is why the excitation current cosine polynomial is of the form

$$i_0(\theta)=\sum_{k=0}^{n}C_k\cos k\theta,\qquad k=0,\ldots n,\qquad \theta=\frac{2\pi}{T}t, \tag{15}$$

where $i_0(\theta)$ meets the requirements of the Theorem I. Then this function is directly transformed into an algebraic polynomial of the form

$$i_0(x)=\sum_{k=0}^{n}C_kT_k(x),\qquad k=0,\ldots n,\qquad x\in[-1,1]. \tag{16}$$

In the case of using the parametric function $\Phi_m\cos\theta$ for the mapping of $[-\pi,0]$ on $\varphi\in[-\Phi_m,\Phi_m]$, the cosine polynomial (15) is directly transformed into the algebraic polynomial of the form

$$\begin{aligned} &i_0(\varphi)=\sum_{k=0}^{n}C_kT_k\left(\frac{\varphi}{\Phi_m}\right),\qquad k=0,\ldots n,\\ &\varphi/\Phi_m=x\in[-1,1],\qquad \varphi\in[-\Phi_m,\Phi_m], \end{aligned} \tag{17}$$

with identical values of the coefficients C_k as in (15), (16) and (17).

This is the main result in the practical application of the Theorem I and its Corollary I (in further text Theorem I) regarding the computing efficiency and approximation accuracy.

5.1 Technical requirements for obtaining Chebyshev nodes and determination of the subsets of samples that represent the nodes of the first and the second kind.

Technical requirements for the successful application of the Theorem I imply the use of the zero crossing sampling system, such as the set of two Agilent 3458 A multimeters that was used in the experimental validation of the Theorem I together with the sinusoidal voltage source Fluke 6100 A with $f = 50$ Hz mains frequency. A single phase transformer 220 V/57.73 V, $S_n = 100$ VA was used as a measuring object for this purpose.

The sampling rate of 10 kHz gives a set of 101 synchronized excitation current and magnetic flux samples across the electric angle segment $\theta\in[-\pi,0]$, ($\theta = 2\pi ft$). The first sample from this set that corresponds to the negative extremum, for both the flux and the excitation current, is indexed with the index value 0. Then, the last sample from this set that corresponds to the positive extremum for both the flux and the excitation current is indexed with the index value 100.

Let the sample index be denoted with k. Then the CHN_I nodes are determined by the expression [18]

$$x_{kChI}=\cos\frac{(2n_{ChI}-2k+1)\pi}{2n_{ChI}},\quad \left(k=1,2,\ldots,n_{ChI}<100\right),\quad \pi=\frac{\omega T}{2}, \tag{18}$$

and the CHN_II nodes are determined by the expression [18]

$$x_{kChII} = \cos\frac{k\pi}{n_{ChII}-1}, \quad \left(k = 0,1,\ldots,n_{ChII}-1 \le 100\right), \quad \pi = \frac{\omega T}{2}. \tag{19}$$

For obtaining the series of ascending sample values for the electric angle segment $\theta \in [-\pi,0]$, the expressions (18) and (19) are to be rearranged into the appropriate form

$$x_{kChI} = \cos\left(-\frac{\left(2n_{ChI}-2k+1\right)\pi}{2n_{ChI}}\right), \quad \left(k = 1,2,\ldots,n_{ChI}\right), \tag{20}$$

and

$$x_{kChII} = \cos\left(\frac{k\pi}{n_{ChII}-1}-\pi\right), \quad \left(k = 0,1,\ldots,n_{ChI}-1\right). \tag{21}$$

Finally, by means of the substitution $\Delta\theta = \pi/100$, where $\Delta\theta$ represents the sampling step, expressions (20) and (21) get the form

$$x_{kChI} = \cos\left(-\frac{\left(2n_{ChI}-2k+1\right)\cdot 100\Delta\theta}{2n_{ChI}}\right), \quad \left(k = 1,2,\ldots,n_{ChI}\right), \tag{22}$$

and

$$x_{kChII} = \cos\left(\frac{k\cdot 100\Delta\theta}{n_{ChII}-1}-\pi\right), \quad \left(k = 0,1,\ldots,n_{ChII}-1\right). \tag{23}$$

Based on (22), the expression for determining index values of the CHN_I nodes is derived

$$k_{ChI} = 100 - \frac{\left(2n_{ChI}-2k+1\right)100}{2n_{ChI}}, \quad \left(k = 1,2,\ldots,n_{ChI}\right). \tag{24}$$

The above expression allows only those values for n_{ChI} that produce the integer values for k_{ChI}. Therefore, n_{ChI} can take only the values from the set $\{50,25,10,5,2,1\}$.

Similarly, from (23) it is obtained

$$k_{ChII} = \frac{k\cdot 100}{n_{ChII}-1}, \quad \left(k = 0,1,\ldots,n_{ChII}-1\right), \tag{25}$$

and integer values for k_{ChII} will be obtained only if n_{ChII} takes values from the set $\{101,51,26,11,6,5,3,2\}$.

In Table 1 are represented all possible index values obtained from the expressions (24) and (25), except for the values for $n_{ChI} \le 5$ and $n_{ChII} \le 6$. The reason for this is that an expected number of excitation current harmonics is certainly higher then 5. In addition, the index values for $n_{ChII} = 101$ are excluded

from the **Table 1**. In the case of $n_{ChII} = 101$, the entire set of samples would be included and thus an analysis of the error distribution could not be possible.

Table 1

Identification of the sample subsets that represent Chebyshev nodes.

for	Index of the sample that coincides with a node index
$n_{ChI} = 10$	{5,15,25,35,45,55,65,75,85,95}
$n_{ChII}=11$	{0,10,20,30,40,50,60,70,80,90,100}
$n_{ChII}=21$	{0,5,10,15,20,25,30,35,40,45,50,55,60,65,70,75,80,85,90,95,100}
$n_{ChI}=50$	{1,3,5,7,9,11,13,15,17,19,21,23,25,27,29,31,33,35,37,39,41,43,45,47,49,51, 53,55,57,59,61,63,65,67,69,71,73,75,77,79,81,83,85,87,89,91,93,95,97,99}
$n_{ChII}=51$	{0,2,4,6,8,10,12,14,16,18,20,22,24,26,28,30,32,34,36,38,40,42,44,46,48,50, 52,54,56,58,60,62,64,66,68,70,72,74,76,78,80,82,84,86,88,90,92,94,96,98,100}

5.2 The discrete orthogonality of the Chebyshev polynomials and two examples of practical application of the Theorem I

An interpolation polynomial over n+1 CHN_I nodes from normalized flux domain segment $x\in[-1,1]$ has the following form [18]

$$i_0(x)=\sum_{k=0}^{n}{}'c_k T_k(x)=\frac{1}{2}c_0 T_0(x)+\sum_{k=1}^{n}c_k T_k(x), \qquad x\in[-1,1]. \tag{26}$$

By virtue of the discrete orthogonality [17, 18] of the Chebyshev polynomials over CHN_I nodes, the c_k coefficients are computed by two equivalent expressions

$$c_k=\frac{2}{n+1}\sum_{j=1}^{n+1} i_0(x_j)\cdot T_k(x_j), \qquad x_j=\cos\left(-\frac{(2(n+1)-2j+1)\pi}{2(n+1)}\right) \tag{27}$$
$$(k=0,\ldots,n), \qquad (n+1=n_{ChI}),$$

and

$$c_k=\frac{2}{n+1}\sum_{j=1}^{n+1} i_0\left(-\frac{(2(n+1)-2j+1)\pi}{2(n+1)}\right)\cdot\cos k\left(-\frac{(2(n+1)-2j+1)\pi}{2(n+1)}\right), \tag{28}$$
$$(k=0,\ldots,n), \qquad (n+1=n_{ChI}).$$

In accordance with (15) and (16) a cosine interpolation polynomial over ±1 CHN_I nodes in the electrical angle domain $\theta\in[-\pi,0]$ has the following form [18]

$$i_0(\theta)=\sum_{k=0}^{n}{}'c_k\cos k\theta=\frac{1}{2}c_0+\sum_{k=1}^{n}c_k\cos k\theta,\qquad \theta\in[-\pi,0]. \tag{29}$$

An example of the Theorem I application by means of (26) – (29) is represented for the set of $n_{chI}=10$ Chebyshev nodes of the first kind in tabulated form in **Table 1** and in graphical form in Fig. 3.

Similarly, n+1 Chebyshev nodes of the second kind have the following expressions [18]:

$$i_0(x)=\sum_{k=0}^{n}{}''c_kT_k(x)=\frac{1}{2}c_0T_0(x)+\sum_{k=1}^{n-1}c_kT_k(x)+\frac{1}{2}c_nT_n(x),\quad x\in[-1,1], \tag{30}$$

$$c_k=\frac{2}{n}\sum_{j=0}^{n}{}''i_0(x_j)T_k(x_j),\qquad x_j=\cos\left(\frac{j\pi}{n}-\pi\right)$$
$$(k=0,\ldots,n),\qquad (n+1=n_{ChII}), \tag{31}$$

$$c_k=\frac{2}{n}\sum_{j=0}^{n}{}''i_0\left(\frac{j\pi}{n}-\pi\right)\cos k\left(\frac{j\pi}{n}-\pi\right),$$
$$(k=0,\ldots,n),\qquad (n+1=n_{ChII}). \tag{32}$$

$$i_0(\theta)=\sum_{k=0}^{n}{}''c_k\cdot\cos k\theta=\frac{1}{2}c_0+\sum_{k=1}^{n-1}c_k\cos k\theta+\frac{1}{2}c_n\cos n\theta,\quad \theta\in[-\pi,0], \tag{33}$$

An example of the Theorem I application by means of (30) – (33) is given for the set of $n_{chII}=11$ Chebyshev nodes of the second kind in tabulated form in **Table 3** and in graphical form in Fig. 4.

Table 2

Cebyshev nodes of the first kind and the coefficients of interpolation polynomial for Chebyshev polynomials basis and for monomials basis.

n_{ChI} node index	sample φ (index) [Wb]	sample φ (index) normalized	sample i_0 (index) [A]	coefficients for Chebyshev polynomial basis		coefficients for monomial x^k basis	
5	-0.0013432231	-0.987688341	-0.117733834	c_0	0.0276080973	a_0	0.019275485
15	-0.0012144271	-0.891006524	-0.071737436	c_1	0.0897163468	a_1	0.015673906
25	-0.0009661704	-0.707106781	-0.020843621	c_2	-0.0095927426	a_2	0.000158380
35	-0.0006214148	-0.453990499	0.006715073	c_3	0.0301421501	a_3	0.057566282
45	-0.0002143542	-0.156434465	0.016626753	c_4	-0.0048764490	a_4	0.045836512
55	0.0002143542	0.156434465	0.021983351	c_5	0.0037755316	a_5	0.065155372
65	0.0006214148	0.453990499	0.033870687	c_6	-0.0003212031	a_6	-0.121367066
75	0.0009661704	0.707106781	0.059072496	c_7	0.0005555446	a_7	-0.053735629
85	0.0012144271	0.891006524	0.090991235	c_8	0.0004339397	a_8	0.055544283
95	0.0013432231	0.987688341	0.119095783	c_9	0.0001550182	a_9	0.039684660

Table 3

Cebyshev nodes of the second kind and the coefficients of interpolation polynomial for Chebyshev polynomials basis and for monomials basis.

n_{ChII} node index	sample φ (index) [Wb]	sample φ (index) normalized	sample i_0 (index) [A]	coefficients for Chebyshev polynomial basis		coefficients for monomial x^k basis	
0	-0.0013594619	-1.0000000000	-0.123795498	c_0	0.0276971868	a_0	0.019154967
10	-0.001294644	-0.9510565163	-0.098412061	c_1	0.0896541475	a_1	0.014298962
20	-0.0011041222	-0.8090169944	-0.044543009	c_2	-0.0095414213	a_2	0.002200856
30	-0.0008038880	-0.5877852523	-0.003735111	c_3	0.0300749038	a_3	0.075706177
40	-0.0004232631	-0.3090169944	0.013030176	c_4	-0.0047526785	a_4	0.048223005
50	0.0000000000	0.0000000000	0.019154967	c_5	0.0036494057	a_5	-0.003897475
60	0.0004232631	0.3090169944	0.026337257	c_6	-0.0000148624	a_6	-0.147501281
70	0.0008038879	0.5877852523	0.045335193	c_7	0.0004456793	a_7	0.045019320
80	0.0011041222	0.8090169944	0.074312542	c_8	0.0004815688	a_8	0.088776878
90	0.0012946439	0.9510565163	0.107005978	c_9	-0.0000286386	a_9	-0.007331486
100	0.0013594619	1.0000000000	0.123795498	c_{10}	-0.0000424001	a_1	-0.010854426

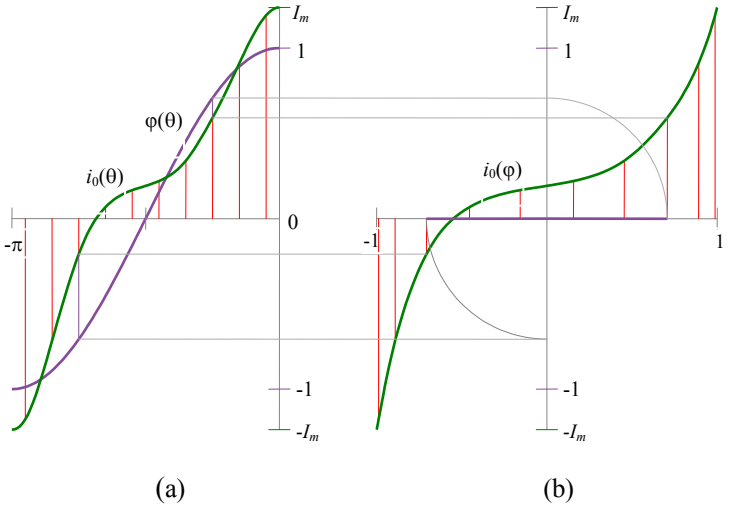

Fig. 3 – (a) *Graph of the cosine interpolation polynomial* $i_0(\theta)$ *over* 10 CHN_I *nodes in the electrical angle domain* $\theta \in [-\pi,0]$; (b) *Graph of the algebraic interpolation polynomial* $i_0(x)$ over 10 CHN_I nodes in normalized flux domain $x \in [-1,1]$.

5.3 Metrological aspects of the Theorem I

Besides the modeling of the dynamic hysteresis loop branches for different purposes, the Theorem I has practical metrology application in determining three parameters of the given magnetic circuit:

1. Coercive current (field),
2. Area of the closed hysteresis loop and
3. Remanence (redsidual) flux.

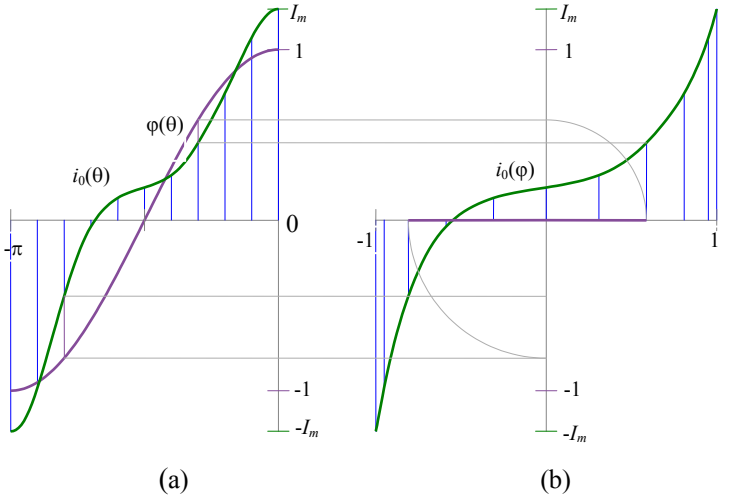

Fig. 4 – (a) *Graph of the cosine interpolation polynomial* $i_0(\theta)$ *over* 11 CHN_II *nodes in the electrical angle domain* $\theta\in[-\pi,0]$. (b) *Graph of the algebraic interpolation polynomial* $i_0(x)$ over 11 CHN_II nodes in normalized flux domain $x\in[-1,1]$.

This is the main reason why the theorem was experimentally validated on a single phase transformer as a measuring object, in order to be applicable without limitation to either the Epstein frame (single sheet or toroidal core specimen), in which case the $H(B)$ interpolation polynomial is to be determined [25, 26], or the arbitrary transformer magnetic circuit where the interpolation polynomial $i_0(\varphi)$ is to be determined.

1. The coercive current (field) determination

In the Fig. 5 is represented the closed dynamic hysteresis loop that consists of the interpolation polynomial $p_{nCh}(0)$ for ascending loop branch and $-p_{nCh}(-x)$, the centrally symmetric to the origin i_0-φ polynomial, for descending loop branch. The polynomial $p_{n_{Ch}}(x)$ has the form of (26) for CHN_I nodes, or (30) for CHN_II nodes [18].

The coercive current is then directly calculated based on

$$i_0(0) = p_{n_{Ch}}(0). \tag{34}$$

By means of the substitution $x = 0$ in (26) for CHN_I nodes, one can get the simple expression (35)

$$i_0(0) = p_{n=n_{Ch}-1}(0) = \frac{1}{2}c_0 + \sum_{i=1}^{[n/2]}(-1)^i c_{2i}, \tag{35}$$

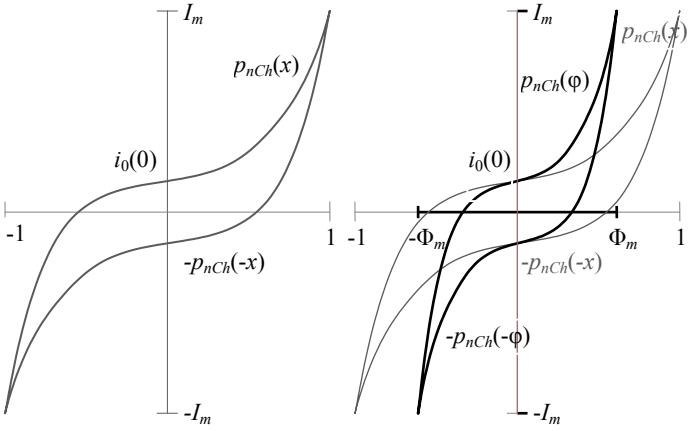

(a) (b)

Fig. 5 – (a) *DHLB's represented by the interpolation polynomials* (16) *on the domain segment* $x \in [-1,1]$; (b) *DHLB's represented by the interpolation polynomials* (17) *on the domain segment* $\varphi \in [-\Phi_m, \Phi_m]$.

and in particular for $n = 9$

$$i_0(0) = p_{n=n_{ChI}-1}(0) = \frac{1}{2}c_0 - c_2 + c_4 - c_6 + c_8. \tag{36}$$

Similarly, based on (30) for CHN_II it holds

$$i_0(0) = p_{n=n_{ChI}-1}(0) = \frac{1}{2}c_0 + \sum_{i=1}^{\left[\frac{n-1}{2}\right]} (-1)^i c_{2i} + (-1)^{\left[\frac{n}{2}\right]} \frac{1}{2} c_{\left[\frac{n}{2}\right]}, \tag{35}$$

and in particular for $n = 10$

$$i_0(0) = p_{n=n_{ChI}-1}(0) = \frac{1}{2}c_0 - c_2 + c_4 - c_6 + c_8 - \frac{1}{2}c_{10}. \tag{36}$$

2. The area of the closed hysteresis loop calculation

When determining the coercive current, it does not matter if the polynomial form of (16) or (17) is used. That is illustrated in Fig. 5. But it is not so obvious for the calculation of an arbitrary closed hysteresis loop area. Namely, it seems that this calculation requires the use of the interpolation polynomial form (17):

$$S_{H_\varphi} = \int_{-\Phi_m}^{\Phi_m} \left(p_{n_{Ch}}(\varphi) + p_{n_{Ch}}(-\varphi) \right) \mathrm{d}\varphi. \tag{37}$$

Integration gives as a result for CHN_I nodes

$$S_{H_\varphi} = 4\Phi_m \left(\frac{c_0}{2} - \sum_{i=1}^{[n/2]} \frac{c_{2i}}{(2i-1)(2i+1)} \right), \tag{38}$$

and in particular for $n = 9$

$$S_{H_\varphi} = 4\Phi_m \left(\frac{c_0}{2} - \left(\frac{c_2}{1\cdot 3} + \frac{c_4}{3\cdot 5} + \frac{c_6}{5\cdot 7} + \frac{c_8}{7\cdot 9} \right) \right). \tag{39}$$

Similarly, the result for CHN_II nodes is

$$S_{H_\varphi} = 4\Phi_m \left(\frac{c_0}{2} - \sum_{i=1}^{[(n-1)/2]} \frac{c_{2i}}{(2i-1)(2i+1)} - \frac{c_{[n/2]}}{2(2[n/2]-1)(2[n/2]+1)} \right), \tag{40}$$

and in particular for $n = 10$

$$S_{H_\varphi} = 4\Phi_m \left(\frac{c_0}{2} - \left(\frac{c_2}{1\cdot 3} + \frac{c_4}{3\cdot 5} + \frac{c_6}{5\cdot 7} + \frac{c_8}{7\cdot 9} \right) - \frac{1}{2}\cdot\frac{c_{10}}{9\cdot 11} \right). \tag{41}$$

The expressions (38) and (40) point out the important fact regarding numerical calculations, that an area of the closed hysteresis loop can be calculated directly on the basis of c_k coefficients and the Φ_m value without the need of generating an interpolation polynomial. The same holds for the determination of the coercive current.

3. The remanence flux determination

Since the polynomial $p_{nCh}(x)$ (16) has only one real zero, the iterative procedure

$$x_{k+1} = x_k - \frac{p_{n_{Ch}}(x_k)}{p'_{n_{Ch}}(x_k)}, \tag{42}$$

gives the value of the normalized remanence flux x_r, and by virtue of x_r is obtained the actual value of the remanence flux φ_r

$$\varphi_r = x_r \Phi_m. \tag{43}$$

5.4 Convergence of an interpolation polynomial to the experimentally obtained DHLB curve and analysis of the error distribution

The measure of approximation accuracy in the case of representing DHLB by using an interpolation polynomial of the form (26) and (30) can be observed by the corresponding error distribution functions

$$e_{n_{ChI}}(x_i) = i_0(x_i) - p_{n_{ChI}}(x_i), \quad i = 0,...,100, \tag{44}$$

and

$$e_{n_{ChII}}(x_i) = i_0(x_i) - p_{n_{ChII}}(x_i), \quad i = 0,...,100. \tag{45}$$

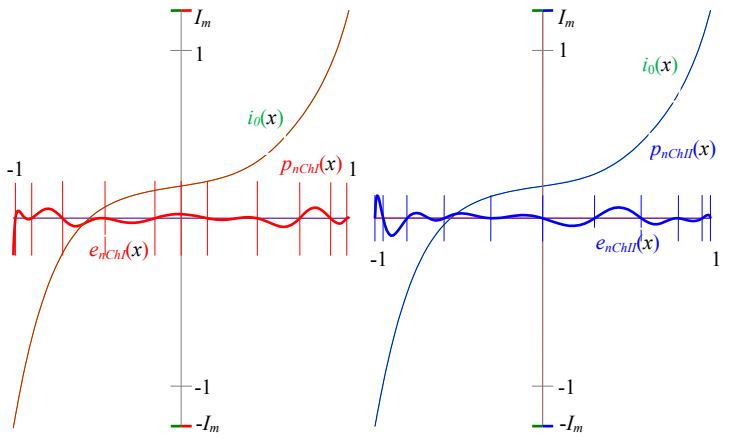

(a) (b)

Fig. 6 – (a) *DHLB and* p_{nChI} *ordinate values are magnified by* 10 times*, whereas* e_{nChI} *ordinate values are magnified by 200 times for* $n_{ChI} = 10$;
(b) *The same holds for DHLB,* p_{nChII} *and* e_{nChII} *ordinate values for* $n_{ChII} = 11$.

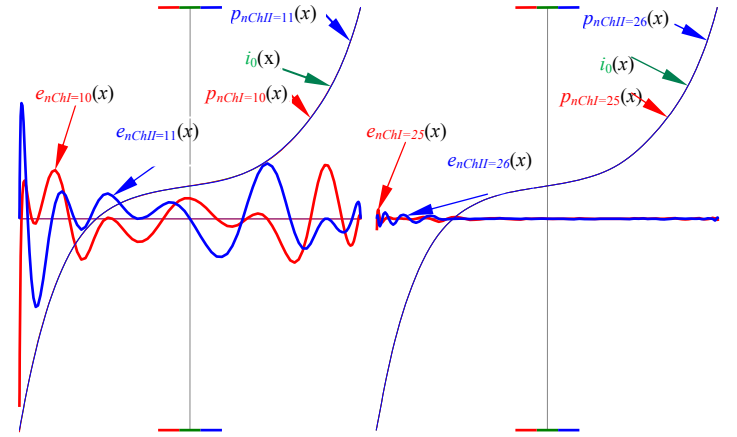

(a) (b)

Fig. 7 – (a) *DHLB,* p_{nChI} *for* $n_{ChI} = 10$ *and* p_{nChII} *for* $n_{ChII} = 11$ *ordinate values are magnified by* 10 *times, whereas* e_{nChI} *for* $n_{ChI} = 10$ *and* e_{nChII}*. for* $n_{ChII} = 11$ *are magnified by* 1000 *times;*
(b) *The same holds for DHLB,* p_{nChI}*,* p_{nChII}*,* e_{nChI} *and* e_{nChII} *for* $n_{ChI} = 25$ *and* $n_{ChII} = 26$.

The graphics of the experimentally obtained DHLB curve are represented in Fig. 6, as well as the interpolation polynomials $p_{nChI}(x)$ and $p_{nChII}(x)$ for

$n_{ChI} = 10$ and $n_{ChII} = 11$, and error distribution functions $e_{nChI}(x)$ and $e_{nChII}(x)$. The ordinate values of the DHLB curve and $p_{nChI}(x)$ and $p_{nChII}(x)$ polynomials are magnified by 10 times, whereas the ordinate values of the error distribution functions $e_{nChI}(x)$ and $e_{nChII}(x)$ are magnified by 200 times.

Apart from the approximation accuracy of an interpolation polynomial, an error distribution function enables the observation of the relationship between the degree of an interpolation polynomial and its convergence to the approximated DHLB. As an illustration of convergence behavior, Fig. 7 represents the graphics of the experimentally obtained DHLB curve and its interpolation polynomials for $n_{ChI} = 10$, $n_{ChII} = 11$, $n_{ChI} = 25$ and $n_{ChII} = 26$ nodes, together with the corresponding error distribution functions. As a result of a very good convergence of the higher degree interpolation polynomial to the DHLB, the magnification of the polynomial ordinate values is retained at 10 times, whereas the ordinate values of the error distribution functions are magnified by 1000 times.

6 Conclusion

An excitation current that fulfils the conditions given in the Theorem I can be accurately approximated by using the cosine polynomial of the form (15), whereas its corresponding DHLB can be approximated by using the corresponding algebraic polynomial of the form (16) i.e. (17), with an equivalent accuracy of approximation for the either normalized or arbitrary magnetic flux amplitude values. From the point of view of metrology, it is important that the above mentioned polynomial can be generated over the discrete subsets of the measured samples, and that an approximation error can be effectively affected by the sampling frequency and the sampling resolution.

The proposed method enables us to express explicitly the DHLB by cosine polynomial in the time (electric angle) domain and by algebraic polynomial in the magnetic flux domain. The earlier represented method of analyzing the hysteresis loops by using the Fourier analysis (Masheva, Geshev and Mikhov [27]) gives an explicit expression of a hysteresis loop branch only for the electric angle domain in the form of a trigonometric polynomial. Actually, the Theorem I defines the conditions for using both of the above mentioned methods. Therefore, a detailed comparative analysis of the approximation efficiency in the dependence of using these two methods over CHN_I and CHN_II nodes should be the subject of the future work.

The presented method can be fully applied on the approximation of the static hysteresis loop branches as well as on the DC magnetization curves. In the absence of the tabulated data relating to the static hysteresis loops or the DC magnetizing curves, the graphical method for obtaining the CHN_I or CHN_II

Chebyshev nodes can be used with no constraints by virtue of the producer catalogues.

7 References

[1] J. A. Ewing: Experimental Researches in Magnetism, Proceedings of the Royal Society of London, Vol. 38, 1884 – 1885, pp. 58 – 62.

[2] E. Madelung: Uber Magnetisierung durch schnellverlaufende Strome und die Wirkungweise der Rutherford-Markoni Magnetodetektors, Annaler der Physik, Vol. 322, No. 10, 1905, pp.861 – 890.

[3] M. P. Langevin: Magnetisme et theorie des electrons, Annales de Chimie et de Physique Vol. 5, 1905, pp. 70 –127.

[4] M.L. Brillouin: Les moments de rotation et le magnetisme dans la mechanique ondulatoire, Journal de Physique et Le Radium, Vol. 8, No. 2, 1927, pp. 74 – 84.

[5] F. Preisach: Uber die magnetishe nachwirkung, Zeitschrift für Physik, Vol. 94, 1935, pp. 277 – 302.

[6] D. C. Jiles, D. L. Atherton: Theory of ferromagnetic hysteresis, Journal of Magnetism and magnetic materials, Vol. 61, 1986, pp. 48 – 60.

[7] J. Fisher, H. Moser: Die nachbildung von magnetisierungscurven durch einfache algebraishe oder transzendente funktionen, Archiv fur Electrotechnik, XLII, No. 5, 1956, pp. 286 –299.

[8] C.F. Trutt, E. A. Erdelyi, R.E. Hopkins: Representation of the Magnetization Characteristic of DC Machines for Computer Use. IEEE Transactions on Power Apparatus and Systems, Vol. PAS–87, No.3, 1968, pp. 665 – 669.

[9] G.F.T. Widger: Representation of Magnetisation Curves Over Extensive Range by Rational Fraction Approximations, Proceedings of IEE, Vol. 116, No.1, January 1969, pp. 156 – 160.

[10] J.R. Brauer: Simple Equations for the Magnetization and Reluctivity Curves of Steel, IEEE Transactions on Magnetics, Vol. 11, No. l, 1975, pp. 81.

[11] J. Rivas, J.M. Zamarro, E. Martin, C. Pereira: Simple Approximation for Magnetization Curves and Hysteresis Loops, IEEE Transactions on Magnetics, Vol. 17, No. 4, 1981, pp.1498 – 1502.

[12] I. D. Mayergoyz: Mathematical Models of Hysteresis and Their Applications, Elsevier Science, Amsterdam, 2003.

[13] G. Bertotti, Hysteresis in Magnetism, Academic Press, San Diego, USA 1998.

[14] A. lvanyi: Hysteresis Models in Electromagnetic Computation, Akademiai Kiado, Budapest, 1997.

[15] E. Della Torre: Magnetic Hysteresis, IEEE Press, New York, USA, 1999.

[16] J. Takacs: Mathematics of Hysteretic Phenomena, Hoboken Wiley/VCH, New York, USA, 2003.

[17] G.M. Phillips: Interpolation and Approximation by Polynomials, Springer–Verlag, New York, USA, 2003.

[18] J.C. Mason, D.C. Handscomb, Chebyshev Polynomials, CRC Press, Washington, D.C, USA, 2003.

[19] D. Jackson: The Theory of Approximation, Chapter IV: Trigonometric Interpolation, pp. 109-148, American Mathematical Society Colloquium Publications, Vol. XI, 1930.

[20] A.E. Fitzgerald, C. Kingsly, S. D. Umans: Electric Machinery, McGraw-Hill, London, 2003.

[21] J.Krstović, R.Radosavljević: Design of distribution transformers, Akademska misao, Belgrade, 2009. (In Serbian).

[22] IEC 60404-2: Methods of measurement of the magnetic properties of electrical steel sheet and strip by means of an Epstein frame IEC Standard Publication, Geneva: IEC Central Office, Switzerland, 1996.

[23] ASTM: A343/A343M-03 Standard Test Method for Alternating-Current Magnetic Properties of Materials at Power Frequencies Using Wattmeter-Ammeter-Voltmeter Method and 25-cm Epstein Test Frame, 2008.

[24] ASTM: A927/A927M-04 Standard Test Method for Alternating-Current Magnetic Properties of Toroidal Core Specimens Using the Voltmeter– Ammeter-Wattmeter Method, 2004.

[25] F. Fiorillo: Measurements of Magnetic Materials, Metrologia, Vol. 47, 2010, S114 – S142.

[26] S. Tumanski: Handbook of Magnetic Measurements, CRC Press, Boca Raton, FL, USA, 2011.

[27] G. Goev, V. Masheva, M. Mikhov: Fourier Analysis of AC Hysteresis Loops, IEEE Transaction on Magnetics, Vol. 39, No. 4, 2003, pp. 1993 – 1996.